Cryoprotectant-free cryopreservation of mammalian cells by superflash freezing

Yoshitake Akiyama (秋山 佳丈)[a,1], Masato Shinose[a], Hiroki Watanabe[a], Shigeru Yamada[b], and Yasunari Kanda[b]

[a]Department of Mechanical Engineering and Robotics, Faculty of Textile Science and Technology, Shinshu University, 3-15-1, Tokida, Ueda, Nagano 386-8567, Japan; and [b]Division of Pharmacology, National Institute of Health Sciences, 3-25-26 Tonomachi, Kawasaki-ku, Kawasaki, Kanagawa 210-9501, Japan

Edited by Robert H. Austin, Princeton University, Princeton, NJ, and approved March 4, 2019 (received for review June 27, 2018)

Cryopreservation is widely used to maintain backups of cells as it enables the semipermanent storage of cells. During the freezing process, ice crystals that are generated inside and outside the cells can lethally damage the cells. All conventional cryopreservation methods use at least one cryoprotective agent (CPA) to render water inside and outside the cells vitreous or nanocrystallized (near-vitrification) without forming damaging ice crystals. However, CPAs should ideally be avoided due to their cytotoxicity and potential side effects on the cellular state. Herein, we demonstrate the CPA-free cryopreservation of mammalian cells by ultrarapid cooling using inkjet cell printing, which we named superflash freezing (SFF). The SFF cooling rate, which was estimated by a heat-transfer stimulation, is sufficient to nearly vitrify the cells. The experimental results of Raman spectroscopy measurements, and observations with an ultrahigh-speed video camera support the near-vitrification of the droplets under these conditions. Initially, the practical utility of SFF was demonstrated on mouse fibroblast 3T3 cells, and the results were comparable to conventional CPA-assisted methods. Then, the general viability of this method was confirmed on mouse myoblast C2C12 cells and rat primary mesenchymal stem cells. In their entirety, the thus-obtained results unequivocally demonstrate that CPA-free cell cryopreservation is possible by SFF. Such a CPA-free cryopreservation method should be ideally suited for most cells and circumvent the problems typically associated with the addition of CPAs.

cryopreservation | superflash freezing | cryoprotectant agent-free | inkjet cell printing | vitrification

Cell cryopreservation is the only method that allows the semipermanent storage of cells without genetic drift by stopping the biological activities in the freezing state (1). Therefore, it is routinely used for the long-term storage of, e.g., conventional cell lines, pluripotent stem cells, spermatozoa, and embryos, all of which may subsequently be used for research and/or clinical purposes. During the freezing process, ice crystals, which are generated inside and outside the cells, can lethally damage the cells (2). Therefore, all conventional cryopreservation methods use at least one cryoprotective agent (CPA) to render water inside and outside the cells vitreous or nanocrystallized (near-vitrification) without forming damaging ice crystals (3). However, CPAs should ideally be avoided due to their cytotoxicity and potential side effects on the cellular state (4, 5). For instance, the acute cytotoxicity of DMSO sometimes induces serious adverse reactions in individual patients (6). DMSO also influences the stemness of embryonic carcinoma cell lines (7) and the differentiation of pluripotent stem-cell lines (8, 9). Less harmful CPAs, e.g., small carbohydrate sugars such as trehalose, may also exhibit cryoprotective effects (10). As the cell membrane is impermeable for these CPAs, a transgenic process is necessary that introduces trehalose into the cytoplasm by expressing trehalose transporters on the cell membrane (11).

Ideally, living cells should be cryopreserved in the same medium as the culture medium. Chemical additives such as CPAs, which might have potential side effects on the cells, should not be contained in the medium. To the best of our knowledge, a CPA-free cell cryopreservation method has not been established yet. However, ideal cryopreservation should theoretically be possible by ultrarapid cooling that is fast enough to vitrify any intra- and extracellular water (12). The minimum cooling rate for the vitrification (critical cooling rates, CCR) for pure water was theoretically estimated to be beyond 3×10^6 °C/s (13), 1×10^7 °C/s (14), or even 1×10^{10} °C/s (15). These CCRs are experimentally unattainable values for droplets of a diameter >10 μm (as, e.g., in cells). Fortunately, complete vitrification is not necessary for cryopreservation, i.e., cells seem to tolerate well the presence of small ice crystals (less than 1 μm) (16). Since the tolerance depends on the CPAs, the tolerance in CPA-free cryopreservation can be expected to be very low. CPA-free cryopreservation should thus be possible in the presence nanocrystallized ice. Taking this tolerance into account, the CCR for cell cryopreservation (CCR_{cell}) should be ~10^4 °C/s. The cooling rate is generally used in cryofixation for microscopy to keep the size of ice crystals <20 nm (17). Therefore, CPA-free cryopreservation (near-vitrification of cells) should also be realized by passing the thermodynamically unstable region between the homogeneous nucleation temperature ($T_h = -38$ °C) and the glass-transition temperature ($T_g = -137$ °C) (18) at a rate faster than the CCR_{cell}.

Herein, we describe a method for the CPA-free cell cryopreservation by superflash freezing (SFF), in which cell suspensions were frozen at rates faster than the CCR_{cell} using inkjet printing techniques. Inkjet printing and spraying of cell suspensions (19–21) have already been applied to ultrarapid freezing in the context of cryopreservation (22–24). However, those studies have aimed at accomplishing high-throughput preservations and lowering the CPA concentration. In the present study, we demonstrate a CPA-free cell cryopreservation technique, in which cell-containing droplets are frozen by reducing their volume to or below 200 pL. Initially, the cooling rate was estimated by a heat-transfer simulation,

Significance

Cryopreservation is routinely used for the long-term storage of cells in various areas of academic, industrial, and clinical research. To keep frozen cells alive, it is necessary to vitrify (or nanocrystallize) water on the inside and outside of the cells. Vitrification is conventionally achieved by adding at least one cryoprotective agent (CPA) to the medium. However, CPAs should ideally be avoided due to their cytotoxicity and potential side effects on the cells. Herein, we demonstrate a method of CPA-free cryopreservation, in which cells are almost vitrified by ultrarapid cooling using inkjet printing. The freezing method should be generally suitable for all kinds of cells that are susceptible to CPAs, including stem cells.

Author contributions: Y.A. designed research; Y.A., M.S., H.W., S.Y., and Y.K. performed research; Y.A. and M.S. analyzed data; and Y.A. and Y.K. wrote the paper.

The authors declare no conflict of interest.

This article is a PNAS Direct Submission.

[1]To whom correspondence should be addressed. Email: aki@shinshu-u.ac.jp.

This article contains supporting information online at www.pnas.org/lookup/suppl/doi:10.1073/pnas.1808645116/-/DCSupplemental.

Published online April 1, 2019.

and the state of droplets frozen by SFF was evaluated by Raman spectrometry and observations with a high-speed camera. Then, we examined whether the SFF method could cryopreserve mouse fibroblast 3T3 cells. The warming rate was also estimated by a simulation similar to that of the cooling rate and both were compared. Finally, the SFF method was applied to other kinds of mammalian cells including stem cells.

Results and Discussion

We developed an inkjet-based SFF system to print very small cell-containing droplets on glass substrates that were cooled with liquid nitrogen (LN) (Fig. 1 *A*–*C*). To obtain maximum cooling rates, we adopted solid-surface vitrification (SSV) (25), i.e., the droplets were not cooled directly by LN, but by the LN-cooled substrate. This indirect cooling method was chosen due to the so-called Leidenfrost effect (26), which describes the formation of a thermally insulating layer of gaseous N_2 from LN upon injecting the droplets directly into LN. Inkjet heads with nozzle diameters of 60 and 40 μm were used, which resulted in the ejection of droplets of ∼200 and 40 pL, respectively (Fig. 1*D*). The volume was determined geometrically based on microscopic images (*SI Appendix*, Fig. S1).

Initially, we confirmed that the cooling rate of the system was sufficient for the near-vitrification of mammalian cells. Given that the droplets are too small to measure the temperature directly with a sensor, the temperatures were estimated by a transient simulation of the heat transfer. We simulated the heat transfer between the droplets and the glass substrates using a 2D axisymmetric model (*SI Appendix*, Fig. S2). The simulations were performed under three conditions: (*i*) 200-pL droplets cooled on thick substrates (thickness: 150 μm), (*ii*) 40-pL droplets cooled on thick substrates (thickness: 150 μm), and (*iii*) 40-pL droplets cooled on thin substrates (thickness: 5 μm) (*SI Appendix*, Fig. S3 and Movie S1). Average cooling rates were calculated from the temperature on the whole droplet in the thermodynamically unstable region. Thus, cooling rates of 7.2×10^3 °C/s (200 pL, thick substrate), 2.2×10^4 °C/s (40 pL, thick substrate), and 3.7×10^4 °C/s (40 pL, thin substrate) were calculated (Fig. 2*A*). The highest cooling rate for the 200-pL droplets (1.6×10^4 °C/s) was obtained in the bottom-right region. Both average cooling rates estimated for the 40-pL droplets were higher than the CCR_{cell}, while the one for 200 pL was almost equal to the CCR_{cell}. Moreover, the cooling rate in the entire area of the 40-pL droplets exceeded the CCR_{cell} (Fig. 2*B*). These results show that CPA-free cryopreservation is theoretically possible for 40-pL droplets.

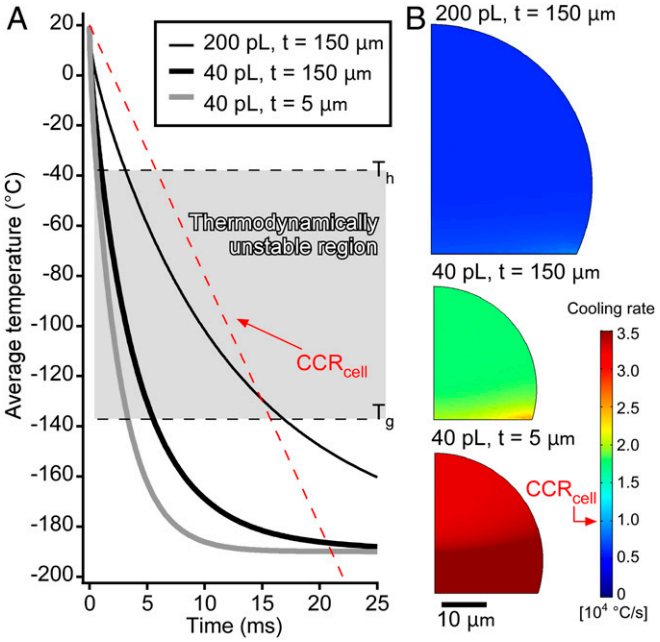

Fig. 2. Estimation of the cooling rates using a heat-transfer simulation. (*A*) Time courses of the average temperatures of the entire droplets. The dashed red line shows cooling for the CCR_{cell} from 20 °C. In the thermodynamically unstable region, the cooling of the 200-pL droplets was slower than the CCR_{cell}, while the cooling of both 40-pL droplets was faster than the CCR_{cell}. (*B*) Contour plots of the average cooling rate of the droplets in the thermodynamically unstable region. The cooling rate anywhere on the 200-pL droplet was less than the CCR_{cell}. Regardless of the thickness of the substrate, the cooling rate on the 40-pL droplets exceeded the CCR_{cell}.

Subsequently, we confirmed the near-vitrification of the droplets experimentally by microscopic Raman spectroscopy. For that purpose, the Raman spectra of SFF-vitrified 200- and 40-pL droplets were compared with that of a 10-μL droplet, which crystallized due to its size. Ice crystals exhibit a strong peak at ∼3,090 cm^{-1} that should be assigned to the OH stretching vibration. Vitrification shifts the peak by ∼20 cm^{-1} toward low-frequency region, which is due to the breakdown of the intermolecular coupling (27, 28). The spectrum of the 10-μL droplet exhibited a peak at 3,091 cm^{-1}, while both spectra of the 200- and 40-pL droplets exhibited a corresponding peak at 3,109 cm^{-1} (Fig. 3*A*). The obtained data indicate that both droplets were at least partially vitrified.

We also evaluated the freezing state using a high-speed camera. Initially, we confirmed that nearly vitrified (vitreous or nanocrystallized) saline is still transparent, whereas crystallized saline is opaque (*SI Appendix*, Fig. S4) (24). Accordingly, the brightness of the droplets should increase only with increasing crystallization of the droplet. The freezing states of the droplets were evaluated by comparing the time courses of the brightness to two control experiments, i.e., a 40-pL droplet including 20 wt % glycerol cooled by the system (vitrification control), and a 40-pL droplet cooled by the system with dry ice instead of LN (crystallization control) (Fig. 3*B* and *SI Appendix*, Fig. S5 and Movie S2). The brightness of the SFF-cooled 200-pL droplet increased for 4 ms after deposition before becoming constant. This period is almost identical to the simulated cooling time at T_h (Fig. 2*A*).

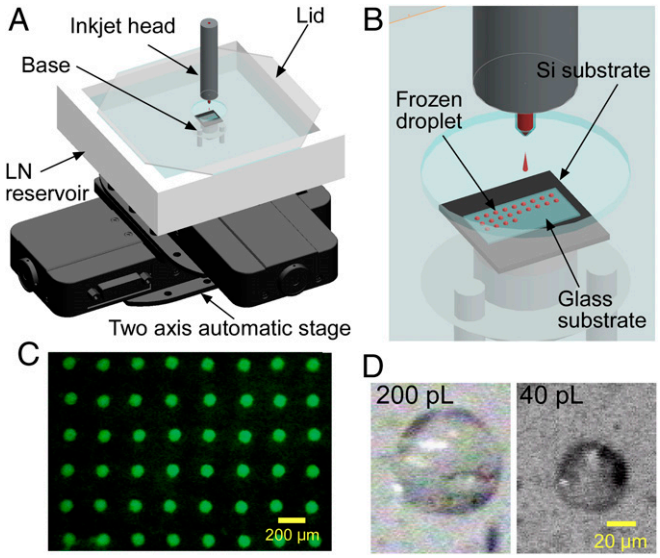

Fig. 1. SFF system for the CPA-free cryopreservation of cells. (*A*) Schematic illustration of the entire system. (*B*) Enlarged illustration of the inkjet head, which is fixed and constantly ejects droplets. The droplets were printed on grid points at intervals of 200 μm by programming the automatic stage. (*C*) Fluorescence image of 200-pL droplets printed on a glass substrate cooled with LN. To visualize the droplets, the culture medium was supplemented with 0.1 mM fluorescein. (*D*) Microscopic images of 200- and 40-pL droplets, observed at an angle of ∼45°.

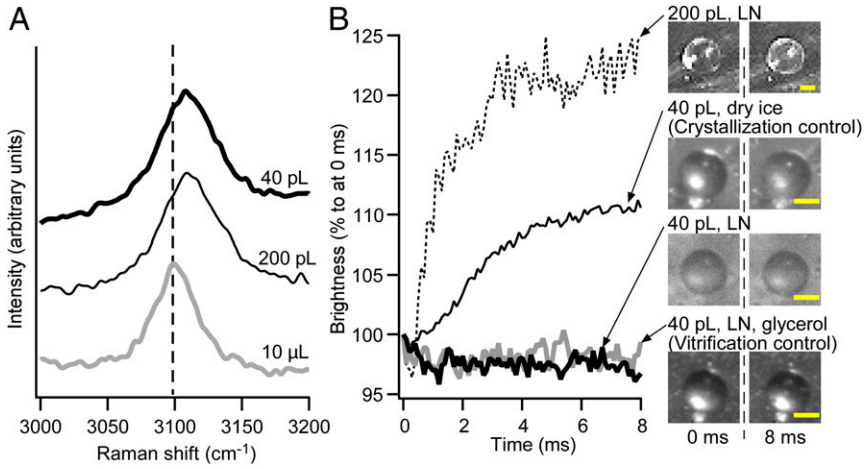

Fig. 3. Experimental assessment of the freezing states of the droplets. (*A*) Raman spectra for 10-μL, 200-pL, and 40-pL droplets. A peak at ~3,100 cm^{-1} was assigned to the OH stretching vibration, which shifts toward the low-frequency region in the vitreous state. The peaks of both inkjet-printed droplets shifted by ~20 cm^{-1} relative to that of the 10-μL droplet (vertical dotted line). (*B*) Time course of the brightness of the droplets frozen under varying conditions. The moment when the droplet was deposited on the substrate was defined as 0 ms. The 200-pL droplet brightened within 3 ms after the deposition. The 40-pL droplet deposited on the substrate that was cooled with dry ice exhibited slightly increased brightness. The 40-pL droplets deposited on the LN-cooled substrate exhibited constant brightness regardless of the presence or absence of glycerol. (Scale bars, 25 μm.)

This result suggests a homogeneous nucleation in the 200-pL droplet. Conversely, the brightness of the SFF-cooled 40-pL droplet remained constant, which suggests that the droplet was nearly vitrified. Considering the results of the Raman spectroscopy measurements and the observations of the high-speed camera, we concluded that the SFF-cooled 40- and 200-pL droplets were nearly vitrified entirely and partially, respectively.

Given the likely vitrification of these droplets, we subsequently evaluated the potential viability of SFF on 3T3 cells, which were frozen and thawed under various conditions (Fig. 4*A*). Before the freezing experiments of the cells, we confirmed that the influence of inkjet ejection on the 3T3 cells was negligible (*SI Appendix*, Fig. S6). Firstly, cells thawed immediately after freezing were examined. As expected, cells slowly frozen in the absence of a CPA were almost completely dead after thawing (29). Although the cells ejected as 200-pL droplets on thick substrates (thickness: 150 μm) survived partially, the survival rate was <25% of that of the conventional cryopreservation method. The survival rate increased drastically upon reducing the droplet size from 200 to 40 pL. The survival rate for 40-pL droplets on thick substrates (thickness: 150 μm) was comparable to that of the conventional method. The usage of thin substrates (thickness: 5 μm) increased the cell viability by another 5%. These results show that the SFF of 40-pL droplets should enable CPA-free cryopreservation with survival rates that offer practical utility.

Apart from the cooling rate, the warming rate also represents an important parameter Recent studies (16, 30, 31) have shown that recrystallization of vitreous water and crystal growth during the warming process can inflict lethal damage on the cells. The transient simulation of the heat transfer for the warming process was also performed (*SI Appendix*, Fig. S7). The medium flow around the droplet and the substrate was ignored since the warming process was also expected to thaw droplets instantaneously. The results are shown in Fig. 5 and Movie S4 and summarized together with the cooling and survival rates in Table 1. The estimated warming rates were approximately three to four times higher than the corresponding cooling rates, whereas the critical warming rates of several solutions were reported to be one to three orders of magnitude higher than the CCR (32). The critical warming rate for cells (CWR_{cell}) was estimated to be 10^5 °C/s, which is one order of magnitude higher than CCR_{cell}. This value is comparable to the highest obtained in this study (40-pL droplet on a thin substrate) and higher than the other conditions. A comparison between the cooling and warming rates suggested that the SFF system achieves sufficiently high cooling rates to nearly vitrify cells, while increasing the warming rate should further improve the SFF method.

Furthermore, the warming rates for 200- and 40-pL droplets with thick substrates drastically decreased in the region around T_h, which might cause the droplet to recrystallize. These results show that the warming rate is easily affected by the thermal capacity of the carrier for the frozen samples (e.g., the glass substrate). Accordingly, the reason why CPA-free cryopreservation has not been accomplished so far might be ascribed to the warming rate rather than to the cooling rate.

Next, the influence of the storage period was evaluated. Theoretically, even samples frozen without CPA must be kept for safety in the vitreous state, i.e., below the T_g. The SFF-frozen cells were cryopreserved in the vapor phase of an LN dewar, which is comparable to the long-term storage of conventional vitrification methods that use high concentrations of CPAs. Even samples that have been frozen by slow-rate-freezing method are

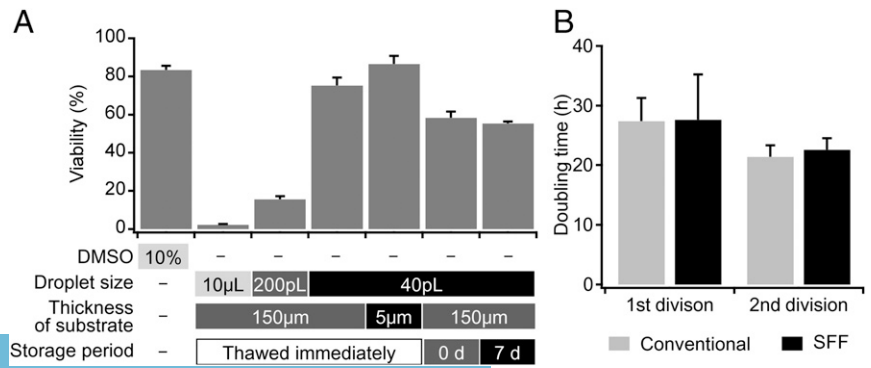

Fig. 4. Comparison of the cell viabilities after thawing under varying conditions. (*A*) Bar 1 was obtained from a conventional freezing method, while bars 2–7 were obtained from the SFF method in the absence of CPAs. The highest viability was obtained from freezing 40-pL droplets on a 5-μm-thick substrate (bar 5). Bars 6 and 7 refer to a method wherein the frozen cells were once transferred to the vapor phase of LN and thawed immediately or 5 d thereafter (n = 5). (*B*) Doubling times for the first and second divisions of 3T3 cells. Both first doubling times were longer than the general doubling time for 3T3 cells (20–24 h). The doubling times of the second divisions were comparable to the general one. A significant difference was not detected for the first and second doubling times between the SFF method and the conventional method (n = 5).

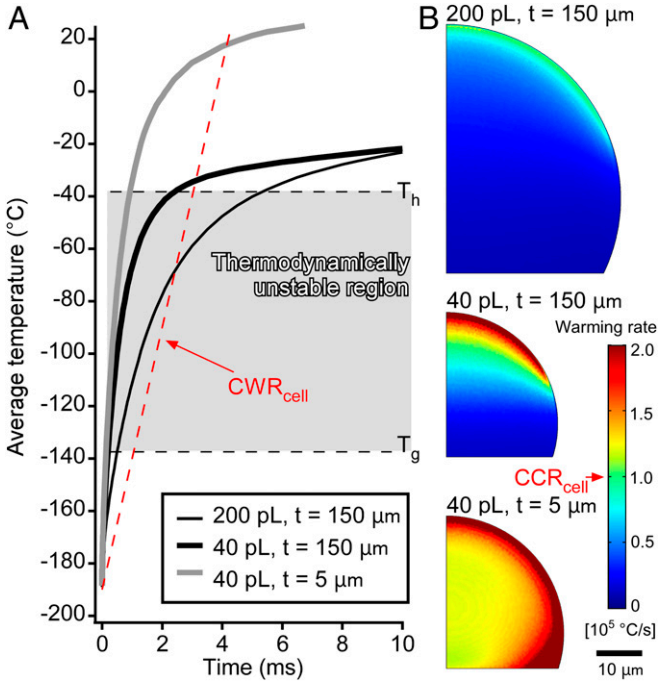

Fig. 5. Estimation of the warming rates using a heat-transfer simulation. (*A*) Time courses of the average temperatures of the entire droplets. The dashed red line shows cooling for the CWR_{cell}. The 40-pL droplet on thin substrate was warmed over the crystalline point at once; on the other hand, the warming rates for the droplets on thick substrates decreased around T_h due to cooling by the substrate. (*B*) Contour plots of the average warming rate of the droplets in the thermodynamically unstable region. The warming rate anywhere on the 40-pL droplet on thin substrates was more than the CWR_{cell}. In the case of thick substrates, less than half of the area of the 40-pL droplet and only part of the 200-pL droplet exhibit a cooling rate over the CWR_{cell}.

usually stored in the same way to maintain their long-term viability. As expected, cell viability by SFF did not decrease during a week of storage (the two right bars in Fig. 4*A*). The division ability of 3T3 cells after a week of storage was assessed based on a time-lapse observation (*SI Appendix*, Fig. S8 and Movie S3). As far as the doubling time is concerned, a difference between the SFF and the conventional method could not be detected (Fig. 4*B*). These results suggest that the SFF-frozen cells can be stored semipermanently below the T_g.

However, the viability can be compromised by transporting the cells into the LN dewar, as evident from the viability of 40-pL droplets on thick substrates (thickness: 150 μm) that were thawed immediately and stored for 0 d (Fig. 4*A*). During the transport of the cells into the cryotube, and the immersion of the cryotube into the LN dewar, devitrification and recrystallization induced by increased temperatures can easily occur. This result indicates that the temperature of SFF-frozen cells must be maintained rigorously, particularly during the transfer process. Due to the extremely small thermal volume, the CPA-free vitrified or nanocrystallized droplets can recrystallize easily upon a brief exposure to atmospheric conditions, i.e., beyond the T_g of water. Therefore, the development of automated SFF systems should keep cells consistently below the T_g of water.

The SFF method was also applied to other cell types [mouse myoblast C2C12 cells and rat mesenchymal stem cells (MSCs)] (33). The viability was evaluated without storage period after freezing 40-pL droplets on thick glass substrate (Fig. 6*A*). The survival rates of both cells were almost identical. Furthermore, MSC characterization after the SFF method was examined. MSCs are known to express a variety of surface epitopes including cell adhesion molecules and enzymes. CD146 is a transmembrane glycoprotein which mediates cell adhesion and is used as a marker of multipotency of MSCs (34). CD73 is ecto-5′-nucleotidase, which is specifically expressed in MSCs, and $CD73^+$ MSCs have been reported to have self-renewal (35). It was confirmed that MSCs frozen by the SFF method still kept expressing the markers for MSCs (Fig. 6*B*). These results show that the SFF method is able to keep not only high cell viability but also cellular state like stemness.

The upper sample-size limit of this method is defined by the diameter of the nozzle of the inkjet head. Empirically, the specimen size should be at least less than one-half of the nozzle diameter to ensure stability of the inkjet injection (e.g., 20 μm for 40-pL droplets). Specifically, samples over 40 pL such as mammalian oocytes (mouse: ∼70 μm; human: ∼120 μm) (36), organoids, and spheroids are thus theoretically inapplicable at the moment. On the other hand, inkjet heads that can eject smaller droplets (<40 pL) can be applied for smaller cells such as sperms and thrombocytes, which might improve the viability.

The SFF method should also find applications in the cryofixation in cellular imaging such as soft X-ray tomography, high-aperture cryolight microscopy, and their combination (37). Cryofixation by plunge freezing is widely used for the sample preparation in these imaging techniques, since it can halt all motion and metabolic activity (38). As far as the resolution is concerned, these imaging methods are not affected by the presence of small ice crystals that might be generated by the SFF method. On the other hand, SFF should not be suitable for cryoelectron microscopy given its high resolution (less than 1 nm).

We have demonstrated a method for a CPA-free cryopreservation that is based on cooling rates that are faster than the CCR_{cell}. The SFF method circumvents two major issues of conventional methods, i.e., the cytotoxicity of the CPA and the dehydration of cells. If the generation of ice crystals is inhibited completely by further increasing the cooling rate, the resulting viability should surpass that of conventional methods. However, the samples must always remain below the T_g of water, as the extremely small thermal volume of the droplets suffers easily from recrystallization by devitrification. Moreover, the mechanical stress exerted on the cells by inkjet printing must be taken into consideration. Nevertheless, the SFF method should be ideally suitable for a broad variety of cells and is expected to be applied soon to pluripotent stem cells and hemocytes for blood transfusion by constructing an automated system.

Methods

Inkjet-Based SFF System. The system is composed of a piezo-based inkjet device (IJK-200H; Microjet), an LN cooling system, and a two-axis automatic stage (SGSP20-85; Sigma Koki) (Fig. 1*A*). The base is made of aluminum and was partially immersed into the LN of the LN reservoir (polystyrene foam). Thick (thickness: 150 μm; C1100; Matsunami Glass) or thin (thickness: 5 μm; C1100, OA-10G; Nippon Electric Glass) glass substrates were stacked on a small piece of Si wafer, which was placed on top of the base (Fig. 1*B*). The LN reservoir was covered with a polymethyl methacrylate lid. The corners of the lid were cut off to let the evaporating nitrogen escape. LN was poured into the LN reservoir a few minutes before starting the inkjet printing. T < −190 °C at the top of the glass substrate was confirmed using a K-type

Table 1. Cooling, warming, and survival rates

Droplet	200 pL	40 pL	40 pL
Substrate	Thick	Thick	Thin
CR, °C/s	7.2×10^3	2.2×10^4	3.7×10^4
WR, °C/s	2.9×10^4	6.5×10^4	1.5×10^5
SR, %	19.6	75.3	86.5
WR/CR	4.0	3.0	4.1

CR, cooling rate; WR, warming rate; SR, survival rate.

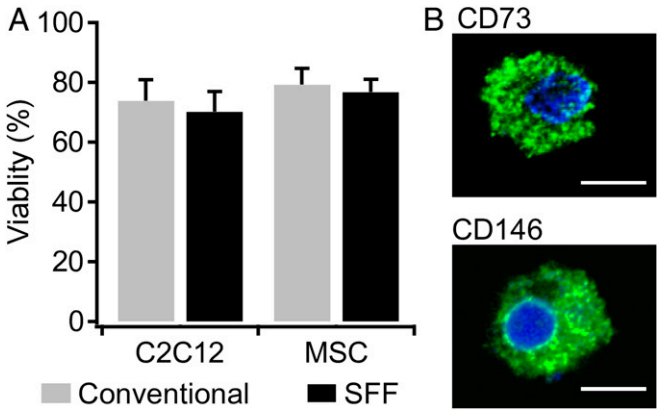

Fig. 6. Cryopreservation of C2C12 cells and MSCs by the SFF method. (*A*) Comparison of cell viability between the SFF method and the conventional method. For the conventional method, cells were frozen by a slow freezing rate with 10% DMSO. In all cases, the viability was over 70%. A significant difference between the methods was not detected ($n = 5$). (*B*) Stemness expression of MSCs frozen by the SFF method. The cells were immunostained with CD73 or CD146 (green) and DAPI (blue). The cells were stained with the stemness marker. (Scale bars, 10 μm.)

thermocouple (KFT-100–200-100; Anbe SMT). When the glass substrate was cooled with dry ice, the temperature was approximately −60 °C on top of the glass substrate. The droplets deposited on the substrate froze instantaneously upon deposition. Detailed conditions for inkjet printing have previously been described elsewhere (19).

A density-adjusted medium was used for inkjet printing to avoid sinking and stacking in the inkjet head (20). The density-adjusted medium was prepared by adjusting the density of the culture medium to 1.045 g/mL with Percoll Plus (17–5445-02; GE Healthcare).

Droplets were printed at intervals of ∼200 μm by synchronizing the inkjet device and the automatic stage with the LabView (National Instruments) software package. While the inkjet head was fixed and droplets were ejected continuously at 50 Hz, the substrate with the LN reservoir moved at 10 mm/s to prevent overlapping of the droplets.

Determination of Droplet Size. The shape and size of the droplets were determined by a zoom microscope (Z16-APO; Leica) and a camera (WAT-221S; Watec). As the droplets were small enough, it was possible to treat the outline of the droplets on the substrate as a circular arc. The actual height h can be obtained from the following equation: $h = r + \cos\theta\{h' - r - r(\cos(\arcsin(h'/r - 1))\tan\theta\}$, where h' is the apparent height, r the radius of the droplet, and θ the observation angle of the camera (*SI Appendix*, Fig. S1). For each inkjet head, five droplets were measured. The inkjet head with a 60-μm diameter ejected droplets of 76.5 μm in diameter and of 54.7-μm height, which affords an approximate volume of 200 pL. The inkjet head with a 40-μm diameter ejected droplets of 48.9-μm radius and 31.8-μm height, which afford an approximate volume of 40 pL. Droplets formed by dropping cell suspensions from a micropipette on the LN cooled glass substrate was also measured (radius: 1.35 mm; height: 1.99 mm), which revealed an approximate volume of 10 μL.

Transient Simulation of the Heat Transfer. A transient simulation was conducted using a finite-element-method–based software (COMSOL). The model consisted of the droplet and the glass (*SI Appendix*, Fig. S3). The aluminum base and the silicon wafer were not taken into account due to their vastly higher thermal conductivity relative to that of the borosilicate glass. Since SFF is an instantaneous phenomenon, convection inside the droplets as well as heat transfer between the droplets and the atmosphere around the droplet were ignored. Specifically, heat could transfer only through the boundary between the bottom line of the droplets and the top line of the glass substrates. The bottom line of the glass substrate was always set to −190 °C, which was the experimentally determined cooling temperature using LN. The other boundaries, except for the axisymmetric ones, were insulated thermally. Furthermore, it was assumed that the droplet at 20 °C was initially deposited on the glass substrate at −190 °C. Phase transitions were not taken into account, as we aimed at stimulating the vitrification. The thermal properties of supercooled and vitrified water are largely unknown. Thus, the thermal properties of supercooled water at −23 °C were used (thermal conductivity: 0.5 W/m·K; density: 983 kg/m^3; heat capacity at constant pressure: 4218 J/kg·K) (39). The thermal properties of the glass substrate were obtained from the literature (40–42). The time-step size was set to 0.02 ms for 0–1 ms, 0.1 ms for 1–20 ms, and 0.5 ms for 20–100 ms. The cooling rate at each point was calculated by differentiating the temperature with respect to time. To draw the contour plot, the cooling rates were averaged during the period in the thermodynamically unstable region. The warming rate was also calculated using a model similar to the one for the cooling rate (*SI Appendix*, Fig. S7). The properties of water given in COMSOL were used for the surrounding medium.

Raman Spectroscopy. Three sizes of droplets (10 μL, 200 pL, and 40 pL) cooled on thick substrates (thickness: 150 μm) were measured. All droplets consisted of the density-adjusted culture medium without phenol red, which increases the background of the Raman spectrum. The first droplets were prepared by dropping the solution with a micropipette on the glass substrate of the SFF system, while the others were prepared by the SFF system using the inkjet head. The droplets on the glass substrate cooled with the LN reservoir were transported with the LN reservoir and set with the LN reservoir on the stage of the Raman spectrometer to inhibit recrystallization of the vitrified water during the measurements. Raman spectra were measured with a Raman microscope (Hololab 5000; Kaiser Optical Systems) using the following measurement conditions: objective lens: 50×, wavelength 531.785 nm, irradiation time 1 s, integration time 1. All recorded spectra were normalized based on the peak intensity at ∼3,100^{-1} cm.

Observations Using a High-Speed Camera. The freezing process of the droplets was observed using a zoom microscope and an ultrahigh-speed camera at 10,000 frames per second (SA-Z or AX200; Photron), which were fixed at 45° relative to the horizontal line. The area around the glass substrate was irradiated with a metal halide illuminator (HIBIKI, HC-M210). The illuminator was turned on only during the observation to prevent the sample from heating. The time course of brightness was evaluated in an area of ∼10 × 10 pixels close to the center of the droplet. The averaged percentages of each initial brightness for three measurements are plotted in Fig. 3*B*.

The freezing state was determined based on a comparison with crystallization and vitrification controls. For the former, a 40-pL droplet of the culture medium was frozen by the SFF system, but the LN chamber was filled with dry ice. Since the temperature of dry ice is higher than the T_g of water, the droplet was absolutely crystallized. In this case, the brightness slightly increased in the first few milliseconds. For the latter, a 40-pL droplet of DMEM including 20 wt % glycerol was frozen by the SFF system. The CCR for a 20 wt % glycerol solution is ∼2.0 × 10^5 K/min (32), i.e., much slower than the cooling rate by the SFF system. The brightness of the droplet was almost constant. These two experiments show that the brightness does not change for the vitrified droplets.

Cell Culture. Mouse NIH 3T3 fibroblast cells and rat myoblast cell line C2C12 were obtained from Riken Cell Bank and American Type Culture Collection, respectively. Rat bone marrow–derived mesenchymal stem cells were obtained as previously reported (33). Dulbecco's modified Eagle medium (DMEM) with high glucose levels (044–29765; Wako Pure Chemical), supplemented with 10 vol/vol % FBS and 1 vol/vol % penicillin-streptomycin solution (168–23191; Wako Pure Chemical) was used as the culture medium for all cells.

Procedures for Freezing and Thawing Cells. During the SFF, the cells were suspended in the density-adjusted culture medium at 1.0 × 10^6 to 10^7 cells per milliliter. The cell suspensions were introduced into the inkjet head thought the nozzle by aspiration from the opposite side of the nozzle. Then, the cells were frozen by the SFF system, and ∼3,000 droplets were ejected onto a glass substrate.

The SFF-frozen cells were thawed rapidly by directly dropping them with the glass substrate into the culture medium (3 mL), which was preheated to 37 °C. Before the experiment, we confirmed that the temperature decrease upon immersing the glass substrate was negligible. When the glass substrate (10 × 10 × 0.15 mm^3) that was cooled to −190 °C was immersed in the culture medium (3 mL, 37 °C), the temperature drop was calculated to be >0.5 °C. To prevent the frozen cells from warming before thawing, we carried the glass substrate on top of the Si substrate by gripping the Si substrate with plastic tweezers that were also precooled by dipping into LN. The thawed cells, which were obtained from several glass substrates, were gathered in a well of 96-well plates (3860–096; AGC Techno Glass) by centrifugation, and cultured therein.

In the conventional cryopreservation method, the cells were suspended (1.0×10^6 cells per millimeter) in the culture medium including 10 vol/vol % DMSO. The cell suspension was deposited in a cryovial and slowly frozen. During the slow freezing, the sample was contained in the freezing vessel (Nihon Freezer), which was placed in a deep freezer (VT-78HC; Nihon Freezer) set to −80 °C. According to the manufacturer's data, the cooling rate is <1 °C/min. After the sample was left for 1 d in the deep freezer, the sample with the cryovial was thawed by immersing in water (37 °C). The cells were washed once with the culture medium to remove any DMSO, and subsequently incubated in the culture medium in a CO_2 incubator.

Evaluation of the Cell Viability. The cell viability was evaluated by live–dead staining, as the cell membrane should be damaged by inkjet printing but recover in a few hours (21). The cells were stained 3 h after thawing. The cells were incubated in the live–dead staining solution (Double Staining Kit CS01; Dojindo) at 37 °C for 30 min. Fluorescence images of the cells were recorded using a fluorescent microscope (DMI IL LED; Leica). The respective numbers of live and dead cells were counted manually and the cell viability was calculated as the ratio between the live cells and all of the cells. When the cells were frozen as 10-μL droplets, the dead cells were uncountable, almost all cells were ruptured. The viability was calculated by dividing the number of live cells by the calculated total cells number included in 10 μL (1.0×10^5).

Time-Lapse Observation of Cells After Thawing. Thawed cells were plated in a well of a 96-well plate and placed in the incubator. The cells were observed with an inverted-phase-contrast microscope (Daiko Science; DSM). Images were taken in intervals of 5 min. Five cells were selected randomly and the doubling times for the first and second divisions were measured. The first and second doubling times are defined as the periods between thawing and the first division, and between the first and second division, respectively.

Immunostaining for MSC Markers. The thawed MSCs were immunostained using the markers CD73 and CD146. Briefly, cells were fixed with 4% paraformaldehyde and permeabilized with 0.2% Triton X-100. The cells were blocked with 5% FBS and incubated overnight at 4 °C with primary antibodies that recognized CD73 (1:200; Abcam) and CD146 (1:500; GeneTex). After rinsing with PBS, the cells were incubated for 1 h at room temperature with Alexa488-conjugated secondary antibody (Thermo Fisher Scientific). Nuclei were counterstained with DAPI (Nacalai Tesque). Fluorescence images were obtained using a Nikon A1 confocal microscope.

Statistical Analysis. Results are represented as mean values ± SD. A comparison for all data was conducted with a Student *t* test, whereby $P < 0.05$ was considered as statistically significant.

ACKNOWLEDGMENTS. The authors thank Dr. Y. Suzuki (National Institute for Materials Science) for discussion on Raman spectra to evaluate the state of water. We thank Dr. S. Yamaguchi and A. Ueno (Microjet) for their technical assistance with inkjet cell printing, as well as M. Hashiguchi (Keisoku Engineering System) for technical assistance with COMSOL simulations. We also thank Y. Suzuki and K. Jo (Photoron) for technical support with the ultrahigh-speed camera, as well as K. Kakegawa (Shinshu University) for help with the Raman spectroscopy measurements. This work was supported in part by Japan Society for the Promotion of Science KAKENHI Grants 25560222, 26709013, and 17K19028 and by the Research Grant on Regulatory Harmonization and Evaluation of Pharmaceuticals, Medical Devices, Regenerative and Cellular Therapy Products, Gene Therapy Products, and Cosmetics from the Japan Agency for Medical Research and Development (JP18mk0104117).

1. Mazur P (1984) Freezing of living cells: Mechanisms and implications. *Am J Physiol* 247:C125–C142.
2. Pegg DE (2015) Principles of cryopreservation. *Methods Mol Biol* 1257:3–19.
3. Galvao J, et al. (2014) Unexpected low-dose toxicity of the universal solvent DMSO. *FASEB J* 28:1317–1330.
4. Best BP (2015) Cryoprotectant toxicity: Facts, issues, and questions. *Rejuvenation Res* 18:422–436.
5. Marx V (2014) Cell-line authentication demystified. *Nat Methods* 11:483–488.
6. Alessandrino P, et al. (1999) Adverse events occurring during bone marrow or peripheral blood progenitor cell infusion: Analysis of 126 cases. *Bone Marrow Transplant* 23:533–537.
7. Kita H, Okamoto K, Kushima R, Kawauchi A, Chano T (2015) Dimethyl sulfoxide induces chemotherapeutic resistance in the treatment of testicular embryonal carcinomas. *Oncol Lett* 10:661–666.
8. Pal R, Mamidi MK, Das AK, Bhonde R (2012) Diverse effects of dimethyl sulfoxide (DMSO) on the differentiation potential of human embryonic stem cells. *Arch Toxicol* 86:651–661.
9. Chetty S, et al. (2013) A simple tool to improve pluripotent stem cell differentiation. *Nat Methods* 10:553–556.
10. Crowe LM, Crowe JH, Rudolph A, Womersley C, Appel L (1985) Preservation of freeze-dried liposomes by trehalose. *Arch Biochem Biophys* 242:240–247.
11. Eroglu A, et al. (2000) Intracellular trehalose improves the survival of cryopreserved mammalian cells. *Nat Biotechnol* 18:163–167.
12. Luyet BJ (1937) The vitrification of organic colloids and of protoplasm. *Biodynamica* 1: 1–14.
13. Bald WB (1986) On crystal size and cooling rate. *J Microsc* 143:89–102.
14. Uhlmann DR (1972) A kinetic treatment of glass formation. *J Non-Cryst Solids* 7: 337–348.
15. Fletcher NH (1971) Structural aspects of the ice-water system. *Rep Prog Phys* 34: 913–994.
16. Huebinger J, et al. (2016) Direct measurement of water states in cryopreserved cells reveals tolerance toward ice crystallization. *Biophys J* 110:840–849.
17. Bald WB (1985) The relative merits of various cooling methods. *J Microsc* 140:17–40.
18. Debenedetti PG (2003) Supercooled and glassy water. *J Phys Condens Matter* 15: R1669–R1726.
19. Yamaguchi S, Ueno A, Akiyama Y, Morishima K (2012) Cell patterning through inkjet printing of one cell per droplet. *Biofabrication* 4:045005.
20. Chahal D, Ahmadi A, Cheung KC (2012) Improving piezoelectric cell printing accuracy and reliability through neutral buoyancy of suspensions. *Biotechnol Bioeng* 109: 2932–2940.
21. Cui X, Dean D, Ruggeri ZM, Boland T (2010) Cell damage evaluation of thermal inkjet printed Chinese hamster ovary cells. *Biotechnol Bioeng* 106:963–969.
22. Zhang X, et al. (2012) Nanoliter droplet vitrification for oocyte cryopreservation. *Nanomedicine (Lond)* 7:553–564.
23. Shi M, et al. (2015) High-throughput non-contact vitrification of cell-laden droplets based on cell printing. *Sci Rep* 5:17928.
24. Dou R, Saunders RE, Mohamet L, Ward CM, Derby B (2015) High throughput cryopreservation of cells by rapid freezing of sub-μl drops using inkjet printing–Cryoprinting. *Lab Chip* 15:3503–3513.
25. Dinnyés A, Dai Y, Jiang S, Yang X (2000) High developmental rates of vitrified bovine oocytes following parthenogenetic activation, in vitro fertilization, and somatic cell nuclear transfer. *Biol Reprod* 63:513–518.
26. Song YS, et al. (2010) Vitrification and levitation of a liquid droplet on liquid nitrogen. *Proc Natl Acad Sci USA* 107:4596–4600.
27. Suzuki Y, Mishima O (2000) Two distinct Raman profiles of glassy dilute LiCl solution. *Phys Rev Lett* 85:1322–1325.
28. Suzuki Y, Mishima O (2003) Raman study of the annealing effect of low-density glassy waters. *J Phys Soc Jpn* 72:3128–3131.
29. Shimada K (1978) Effects of cryoprotective additives on intracellular ice formation and survival in very rapidly cooled HeLa cells. *Contrib Inst Low Temp Sci* B19:49–69.
30. Seki S, Mazur P (2008) Effect of warming rate on the survival of vitrified mouse oocytes and on the recrystallization of intracellular ice. *Biol Reprod* 79:727–737.
31. Mazur P, Seki S (2011) Survival of mouse oocytes after being cooled in a vitrification solution to -196°C at 95° to 70,000°C/min and warmed at 610° to 118,000°C/min: A new paradigm for cryopreservation by vitrification. *Cryobiology* 62:1–7.
32. Hopkins JB, Badeau R, Warkentin M, Thorne RE (2012) Effect of common cryoprotectants on critical warming rates and ice formation in aqueous solutions. *Cryobiology* 65:169–178.
33. Kanda Y, Hinata T, Kang SW, Watanabe Y (2011) Reactive oxygen species mediate adipocyte differentiation in mesenchymal stem cells. *Life Sci* 89:250–258.
34. Russell KC, et al. (2010) In vitro high-capacity assay to quantify the clonal heterogeneity in trilineage potential of mesenchymal stem cells reveals a complex hierarchy of lineage commitment. *Stem Cells* 28:788–798.
35. Suto EG, et al. (2017) Prospectively isolated mesenchymal stem/stromal cells are enriched in the $CD73^+$ population and exhibit efficacy after transplantation. *Sci Rep* 7: 4838.
36. Griffin J, Emery BR, Huang I, Peterson CM, Carrell DT (2006) Comparative analysis of follicle morphology and oocyte diameter in four mammalian species (mouse, hamster, pig, and human). *J Exp Clin Assist Reprod* 3:2.
37. McDermott G, Le Gros MA, Knoechel CG, Uchida M, Larabell CA (2009) Soft X-ray tomography and cryogenic light microscopy: The cool combination in cellular imaging. *Trends Cell Biol* 19:587–595.
38. Harkiolaki M, et al. (2018) Cryo-soft X-ray tomography: Using soft X-rays to explore the ultrastructure of whole cells. *Emerg Top Life Sci* 2:81–92.
39. Sansinena M, Santos MV, Zaritzky N, Chirife J (2011) Numerical simulation of cooling rates in vitrification systems used for oocyte cryopreservation. *Cryobiology* 63:32–37.
40. Childs GE, Ericks LJ, Powell RL (1973) *Thermal Conductivity of Solids at Room Temperature and Below: A Review and Compilation of the Literature* (National Bureau of Standards, Washington, DC), Vol 623, pp 525–530.
41. Yamashita I, et al. (2001) Low-temperature heat capacity of sodium borosilicate glasses at temperatures from 13 K to 300 K. *J Chem Thermodyn* 33:535–553.
42. Sciver SWV (2012) *Low-Temperature Materials Properties, Helium Cryogenics* (Springer, New York), pp 17–58.